Environmental Pollution 285 (2021) 117444

Contents lists available at ScienceDirect

Environmental Pollution

journal homepage: www.elsevier.com/locate/envpol

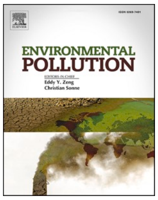

Ozone and SOA formation potential based on photochemical loss of VOCs during the Beijing summer[☆]

Junlei Zhan[a], Zeming Feng[a], Pengfei Liu[b,d,e], Xiaowei He[b,e], Zhouming He[b,e], Tianzeng Chen[b,d,e], Yafei Wang[c], Hong He[b,d,e], Yujing Mu[b,d,e], Yongchun Liu[a,*]

[a] Aerosol and Haze Laboratory, Advanced Innovation Center for Soft Matter Science and Engineering, Beijing University of Chemical Technology, Beijing, 100029, China
[b] Research Center for Eco-Environmental Sciences, Chinese Academy of Sciences, Beijing, 100085, China
[c] Beijing Institute of Petrochemical Technology, Beijing 102617, China
[d] Center for Excellence in Regional Atmospheric Environment, Institute of Urban Environment, Chinese Academy of Sciences, Xiamen 361021, China
[e] University of Chinese Academy of Sciences, Beijing 100049, China

ARTICLE INFO

Keywords:
Photochemical loss
Volatile organic compounds
Photochemical initial concentrations
O_3 pollution
Organic aerosol pollution

ABSTRACT

Volatile organic compounds (VOCs) are easily degraded by oxidants during atmospheric transport. Therefore, the contribution of VOCs to ozone (O_3) and secondary organic aerosol (SOA) formation at a receptor site is different from that in a source area. In this study, hourly concentrations of VOCs and other pollutants, such as O_3, NOx, HONO, CO, and $PM_{2.5}$, were measured in the suburbs (Daxing district) of Beijing in August 2019. The photochemical initial concentrations (PICs), in which the photochemical losses of VOCs were accounted for, were calculated to evaluate the contribution of the VOCs to O_3 and SOA formation. The mean (±standard deviation) measured VOC concentrations and the PICs were 11.2 ± 5.7 and 14.6 ± 8.4 ppbv, respectively, which correspond to O_3 formation potentials (OFP) of 57.8 ± 26.3 and 103.9 ± 109.4 ppbv and SOA formation potentials (SOAP) of 8.4 ± 4.1 and 10.3 ± 7.4 $\mu g\ m^{-3}$, respectively. Alkenes contributed 80.5% of the consumed VOCs, followed by aromatics (13.3%) and alkanes (6.2%). The contributions of the alkenes and aromatics to the OFP_{PICs} were 56.8% and 30.3%, respectively; while their corresponding contributions to the $SOAP_{PICs}$ were 1.9% and 97.3%, respectively. The OFP_{PICs} was linearly correlated with the observed O_3 concentrations ($OFP_{PICs} = 41.5 + 1.40 \times c_{O3}$, $R^2 = 0.87$). The O_3 formation was associated with a VOC-limited regime at the receptor site based on the measured VOCs and changed to a transition regime and a NOx sensitive regime based on the PIC. Our results suggest that more attention should be paid to biogenic VOCs when studying O_3 formation in summer in Beijing, while the control of anthropogenic aromatic compounds should be given priority in terms of SOA formation.

1. Introduction

Atmospheric pollution including particulate matter (PM) and surface ozone (O_3), has received intense attention worldwide, due mainly to their adverse effects on human health (Streets et al., 2007; Krizan et al., 2011). As an important contributor to PM, secondary organic aerosols (SOAs) are formed through the photochemical oxidation of volatile organic compounds (VOCs) and condensation of subsequent organic compounds of low volatility (Han et al., 2017). Tropospheric O_3 is produced via complex photochemistry between VOCs and nitrogen oxides (NOx), during which alkyl peroxide radicals (RO_2) and hydrogen peroxide radicals (HO_2) efficiently convert NO to NO_2, subsequently leading to the net accumulation of O_3 (Chameides et al., 1992). VOCs are precursors of both SOAs and O_3 in the atmosphere (Odum et al., 1997; Carter, 2010).

The O_3 formation potential (OFP) and secondary organic aerosol formation potential (SOAP) are widely used to evaluate the relative contributions of VOC species and sources to ambient O_3 and SOA formation, respectively (Alvim et al., 2018; Kumar et al., 2018; Mozaffar et al., 2020). In practice, the measured VOC concentrations are directly used to calculate the OFP or SOAP (Zheng et al., 2021). However, the VOC concentration and composition observed at a receptor site are likely to be different from those observed in the source region due to the photochemical degradation of VOCs during transport (Warneke et al.,

---

[☆] This paper has been recommended for acceptance by Admir C. Targino.

[*] Corresponding author.
E-mail address: liuyc@buct.edu.cn (Y. Liu).

https://doi.org/10.1016/j.envpol.2021.117444
Received 20 February 2021; Received in revised form 17 May 2021; Accepted 20 May 2021

2004). Both O_3 and SOA formation are related to the consumed VOCs, which react with oxidants, such as OH, NO_3, and O_3. OH is one of the essential oxidants and dominates the degradation of VOCs in the atmosphere, subsequently playing an important role in O_3 (Tan et al., 2018) and SOA formation (Wu et al., 2020). Makar et al. (1999) found that the isoprene concentration was underestimated in models by 40% when the degradation of isoprene by OH radicals was ignored in a one-dimensional canopy model. Gao et al. (2021) found that the emission ratios of highly reactive alkenes were larger than those previously reported in industrial zones when the photochemical loss was considered. Therefore, it is necessary to investigate the differences between the source concentration and the receptor site concentration of VOCs, and its effect on the OFP and SOAP.

The concept of source concentration is similar to that of the photochemical initial concentration (PIC) proposed by Shao et al. (2011), which is based on the photochemical-age approach and has been applied to evaluate the effect of photochemical processing on measured VOC levels. If the emissions of primary VOCs are assumed to be constant, and the influence of fresh emissions during transport is neglected (Roberts et al., 1984; Bertman et al., 1995), the photochemical loss of VOCs during atmospheric transport can be calculated using a ratio method. This method calculates the evolution of the ratio between two VOCs with differences in k_{OH} and has been successfully applied to evaluate the performance of stringent air-quality control measures imposed during the Beijing Olympics (Shao et al., 2011). Shao et al. (2011) found that reduced emissions from gasoline vehicles explained 59–68% of the reduction in the OFPs and suggested that the consumption-based OFP was better than the measurement-based OFP for identifying the key reactive species in local O_3 formation. Yuan et al. (2013) used the photochemical-age-based method to calculate VOC emission ratios in Changdao, and the calculated results were in good agreement with the emission inventory. Han et al. (2017) used this method to estimate the SOA production ratio and compared the characteristics of the VOCs and the formation of SOAs between haze and haze free days in Shanghai. However, this method is rarely used to study the impact of PICs on O_3 and SOA formation in suburban areas because O_3 pollution usually occurs in summer while PM pollution occurs in winter (Ma et al., 2021; Wu et al., 2021). Recently, O_3 and PM pollution occurred simultaneously in summer in Beijing (Duan et al., 2020; Li et al., 2021), highlighting the need to synergistically control O_3 and PM pollution in China.

O_3 concentrations in urban Beijing have exhibited a significant upward trend from May to September, over the period 2001–2015 (Tang et al., 2009; Zhang et al., 2015; Cheng et al., 2018). Moreover, the contribution of the SOA fraction to $PM_{2.5}$ increased by around 1.5 times in the summer of 2015 compared with that in 2008 (Duan et al., 2020). As a result, it is necessary to identify the crucial VOC species that govern the summertime O_3 and SOA formation in Beijing. In this study, we calculated the PIC and assessed the consumption-based O_3 and SOA formation potential in summer in Beijing. The differences between the consumption-based OFP and SOAP and the observation-based values were investigated. The results of this study improve our understanding of the complex photochemistry and provide a scientific basis for efficiently and simultaneously reducing both PM and O_3 pollution in Beijing.

2. Material and methods

2.1. Sampling site description

The sampling site (39.73°N, 116.33°E) is located on the Qingyuan campus of the Beijing Institute of Petrochemical Technology (BIPT) (Fig. 1) and has been described in our previous work (Chen et al., 2020). Briefly, the instruments were installed in a temperature-controlled room on the top floor of a nine-story building (about 27 m above the ground), approximately 600 m from two adjacent streets (Xinghua Street in north-south direction, and Qingyuan Street in east-west direction). The sampling site is a representative suburban site (Chen et al., 2020). Ambient air was drawn through a Teflon manifold (BMET-S, Beijing Saak-Mar Environmental Instrument Ltd.) from the roof using a bypass pump for gas phase pollutant measurements; while particulate matter

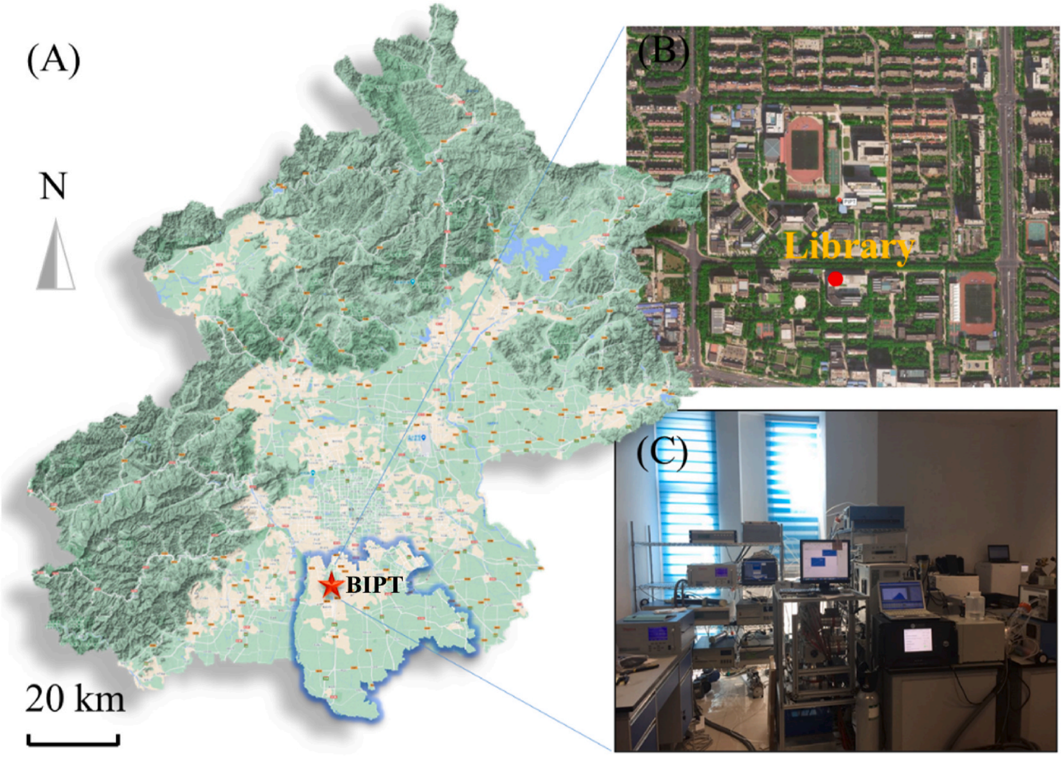

Fig. 1. (A) Map of Beijing, (B) Sampling site and (C) a photograph of the laboratory.

was sampled through a $PM_{2.5}$ inlet with polished steel tubing using a bypass pump (16.7 L min^{-1}).

2.2. Instrumentation

Due to the active photochemistry and low rainfall frequency in August, the observations were carried out from August 1 to 28, 2019. The concentrations of non-methane hydrocarbons (NMHCs) were continuously measured using a custom-built gas chromatography flame ionization detector (GC-FID) system, with a time resolution of 1 h. The details of the analytical procedure have been described by Liu et al. (2016). Briefly, the GC-FID system consisted of a cooling unit, a sampling unit, a separation unit, and an FID, operated at 250 °C. A 400 mL sample of air was collected using a CarbopackTM B sorbent (60/80 mesh) filled stainless-steel tube at a flow rate of 40 mL min^{-1}. Then, the adsorption tube was quickly heated to 180 °C for desorbing and injecting the NMHCs into a single column (OV-1, 30 mL × 0.32 mm I. D.) for separation. The temperature of the capillary column (starting at 60 °C) was held at 60 °C for 3 min, increased to 20 °C at the rate of 12 °C min^{-1}, increased to 30 °C at the rate of 6 °C min^{-1}, increased to 170 °C at the rate of 10 °C min^{-1}, and then held for 2 min. The C2–C12 NMHCs were quantified using external standard curves derived for 57 NMHCs in gas mixtures balanced with N_2 (Spectra Gases Inc., USA) in the range of 1.0–30.0 ppbv. The R^2 values of the calibration curves were 0.99 for all of the NMHCs, and the GC-FID was calibrated weekly. The variations in the responses of the target species were within 6% of the calibration curve. The method detection limits (MDLs) for the NMHCs ranged from 0.02 to 0.10 ppbv, with relative standard deviations (RSD) of 0.3–4.4% (Liu et al., 2016).

NOx, SO_2, CO, and O_3 analyzers (42i, 43i, 48i, and 49i, respectively, Thermo Scientific™, USA) were used to measure the concentrations of the corresponding trace gases. A custom-built long path absorption photometer (LOPAP) was used to measure the HONO concentration (Liu et al., 2020c). Briefly, the HONO in ambient air was absorbed using a solution containing 0.06 M sulfnilamide and 1 M HCl, to which *N*-(1-naphthyl) ethylene-diaminedihydrochloride (0.8 mml L^{-1}) was added to generate an azo dye. The azo dye was detected in a Teflon absorption cell (Liquid Core Waveguide, Biogeneral, USA) using a mini-spectrometer with a diode array detector (SD2000, Ocean Optics, USA). The HONO concentration was obtained by subtracting the calibrated signal of the second coil from the first coil and calibrated using external standard nitrile solutions.

The $PM_{2.5}$ mass concentration was measured using a tapered element oscillating microbalance (TEOM-1405DF, Thermo Scientific™, USA). A High-Resolution Time-of-Flight Aerosol Mass spectrometer (HR-TOF-AMS, Aerodyne, USA), which was alternately operated in V-mode and W-mode, was used to measure the composition of the $PM_{1.0}$. The details have been described in our previous work (Chen et al., 2020). Briefly, the aerosol particles were focused into a tight beam through an aerodynamic lens and were thermally vaporized at 600 °C. The vapors were ionized via electron impact (EI, 70 eV) and were detected using a TOF-AMS detector. The data were analyzed using the PIKA 1.16I software. A collection efficiency (CE) factor of 0.5 and relative ionization efficiency (RIE) values of 1.1, 1.2, 1.4, and 1.3 for NO_3^-, SO_4^{2-}, organic aerosol (OA), and Cl^-, respectively, were used (Chen et al., 2020). A weather station (AWS310, Vaisala, Finland) was used to measure the meteorological variables, including the temperature (T), pressure (P), relative humidity (RH), wind speed (WS), and wind direction (WD). A J_{NO2} filter-radiometer (J_{NO2} radiometer, Metcon, Germany) was used to measure the photolysis rate (J_{NO2}) by continuously measuring the actinic flux in the wavelength range of 285–375 nm.

2.3. Calculation of photochemical loss of VOCs

The photochemical loss of VOCs was calculated using the ratio method (Shao et al., 2011; Yuan et al., 2013). Changes in VOC concentrations as a function of time due to photochemical reaction are described in Eq. (1), from which the OH exposure can be calculated as:

$$\int_0^t c_{OH}dt = \frac{1}{k_{A,OH}-k_{B,OH}}\left[ln\left(\frac{c_A}{c_B}\right)_0 - ln\left(\frac{c_A}{c_B}\right)_t\right] \tag{1}$$

where $(c_A/c_B)_0$ and $(c_A/c_B)_t$ are the emission ratio and the measured ratio of compound A to compound B, respectively; $k_{A,OH}$ and $k_{B,OH}$ are the second-order reaction rates of compound A to compound B, respectively. Thus, for any VOC_i, the PIC is calculated using Eq. (2).

$$c_{i,0} = \frac{c_{i,t}}{exp(-k_{i,OH})exp\left(\frac{1}{k_{A,OH}-k_{B,OH}}\left[ln\left(\frac{c_A}{c_B}\right)_0 - ln\left(\frac{c_A}{c_B}\right)_t\right]\right)} \tag{2}$$

and the photochemical loss of VOC is calculated using Eq. (3).

$$\Delta c_i = c_{i,t}\left[\frac{1}{exp(-k_{i,OH})exp\left(\frac{1}{k_{A,OH}-k_{B,OH}}\left[ln\left(\frac{c_A}{c_B}\right)_0 - ln\left(\frac{c_A}{c_B}\right)_t\right]\right)} - 1\right] \tag{3}$$

In this study, the ethylbenzene/xylene pair was used to calculate ambient OH exposure (Shao et al., 2011; Zheng et al., 2021). Justification for the use of ethylbenzene and xylene is as follows. Firstly, the concentrations of xylene and ethylbenzene are well correlated, which indicates that they are simultaneously emitted (Fig. S1); Secondly, the k_{OH} values of ethylbenzene and xylene are 7×10^{-12} and 1.87×10^{-11} cm^3 $molecule^{-1}$ s^{-1}, respectively (Atkinson and Arey, 2003), which indicates that they have different degradation rates; Finally, the PICs calculated using the ethylbenzene/xylene pair are in good agreement with those calculated using other tracers, such as *i*-butene/propene (Fig. S2). The hourly concentrations of ethylbenzene and xylene were used to calculate the photochemical loss of VOCs. Then, the PIC was calculated by adding the measured VOC concentration and the calculated photochemical loss. In addition to OH exposure, atmospheric transport may also affect the VOC ratio. Sensitivity tests showed that the uncertainty caused by the OH exposure (from −25% to +25%) ranged from 0.77 to 1.33 (Table S1).

2.4. Calculation of OFP and SOAP

Different VOC species have different O_3 formation potentials, which are determined by reaction kinetics and associated mechanisms (Atkinson and Arey, 2003). The OFP has been used to evaluate the contribution of VOCs to O_3 formation in the troposphere, and subsequently, reactivity-based control approaches, which utilize the maximum incremental reactivity (MIR) values of each VOC species (Carter, 2010), i.e. Eq. (4).

$$OFP = \sum(c_i MIR_i) \tag{4}$$

where c_i is the measured concentration of VOC *i*; and MIR_i is the maximum incremental reactivity of VOC *i*.

Similar to the OFP, the SOAP can also be estimated according to the equation (5) (Derwent et al., 2010).

$$SOAP = \sum(c_i SOAP_i) \tag{5}$$

Thirty-nine VOC species with $SOAP_i$ values available in the literature were selected for the SOAP calculations in this study. The $SOAP_i$ represents the potential of a VOC species to form SOA relative to the same mass of toluene when it is added to the ambient atmosphere.

2.5. Box model for O_3 production rate calculations

The O_3 production rates were simulated using a box model with the master chemical mechanism (MCM 3.3.1) (Jenkin et al., 2017). The diurnal curves of the O_3 concentration and production rate were calculated with the initial concentrations of propylene-equivalent VOC and NO_x, which were constrained by the hourly mean values of temperature, relative humidity, pressure, J_{NO2}, and concentrations of CO, SO_2, and HONO during our observations. The measured VOC concentrations were converted to equivalent concentrations of propene according to the MIR values (Zhang et al., 2020b). Isopleths (i.e., empirical kinetic modeling approach, EKMA curves) were drawn based on the daily maximum O_3 production rate. It should be noted that HONO can significantly promote O_3 formation, and its concentration was considered in the model simulations (Zhang et al., 2016).

3. Results and discussion

3.1. Overview of air pollution during observations

Fig. 2 shows the time series of air pollutant concentrations and the meteorological variables during the campaign. The temperature ranged from 21.4 to 34.4 °C, with a mean value (±standard deviation) of 27.4 ± 2.8 °C, and the RH was 18.4%–93.0%, with a mean value of 57.3 ± 19.1%. The mean wind speed was 1.7 ± 1.1 m s^{-1} (ranged from 0.3 to 6.8 m s^{-1}), and the wind was predominantly from the southeast and southwest directions. The mean O_3 concentration during the observation period was 44.8 ± 27.2 ppbv, with a maximum of 119.1 ppbv, which is generally consistent with the mean O_3 concentration (49.1 ± 29.1 ppbv) during 2014–2018 (Maji et al., 2020). The mean $PM_{2.5}$ concentration was 17.4 ± 21.4 μg m^{-3}, which was nearly within Grade II of the Chinese national ambient air quality standard (35 μg m^{-3}). Compared to 2014, in the suburban area, the concentration of $PM_{2.5}$ decreased by 80.3% (Maji et al., 2020), reflecting the effectiveness of air pollution control policies in Beijing. When the wind speed is less than 2 m s^{-1}, local emissions followed by chemical transformation are usually the most important contributors to air pollution in Beijing (Wang et al., 2010). However, light PM pollution still occurred sometimes. O_3 and $PM_{2.5}$ pollution often occurred simultaneously (Fig. 2A and B) when the air masses originated from the south and wind speed was greater than 2 m s^{-1} (Fig. 2F). From August 6 to 9 and from August 18 to 21, the pollutant concentrations (VOCs, $PM_{2.5}$, and O_3) increased substantially. Several O_3 pollution events occurred along with strong southwest wind after August 19. This suggests that regional transport also played important role in the accumulation of O_3 at higher wind speed during these periods.

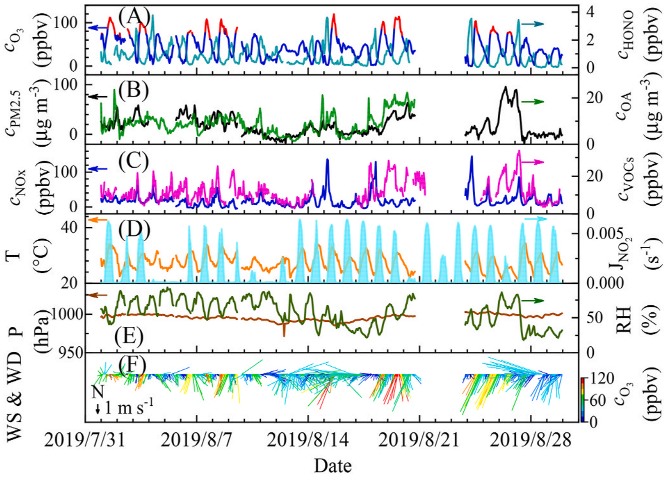

Fig. 2. Time series of the concentrations of O_3, HONO, $PM_{2.5}$, OA, NOx, VOCs, J_{NO2} and the meteorological variables including temperature, relative humidity, wind speed (WS), wind direction (WD), and atmospheric pressure observed in August in Beijing. (In A, the red parts of the c_{O3} indicate the O_3 concentration exceeded 74.6 ppbv according to the second level of the Chinese national ambient air quality standard.)

The concentration of VOCs was weakly correlated with those of OA (R^2 = 0.30) and $PM_{2.5}$ (R^2 = 0.40), but was not correlated with the O_3 concentration (R^2 = 0.05). This can be explained by the differences in the sources and/or formation mechanisms of OA and O_3. As an important component of $PM_{2.5}$, OA accounts for 20–90% of the mass of the $PM_{2.5}$ in the troposphere (Jimenez et al., 2009). In our study, the OA in the $PM_{1.0}$ contributed 46.7 ± 20.5% to the $PM_{2.5}$ mass concentrations, and SOA contributed 72 ± 17% to the OA mass concentrations during our observations. This value is consistent with previous results, i.e., SOA accounted for 74% of the OA concentrations in Beijing in the summer of 2015 (Duan et al., 2020).

In addition to the contributions of secondary sources, primary emissions and other particle components also complicate the observed variations in $PM_{2.5}$ concentration. The O_3 concentration usually reaches a periodic peak in the early afternoon due to the active photochemical reactions under high temperature and solar radiation conditions (Lu et al., 2019). VOCs can break the dynamic equilibrium of NO–O_3–NO_2 and promote the conversion of NO to NO_2, finally leading to an accumulation of O_3. The O_3 concentration is nonlinearly dependent on the VOC concentration. As is shown in Fig. 2A and C, the VOC concentration was usually lower when the O_3 concentration was higher than the second level of the national air quality standard (the red parts in Fig. 2A). Thus, in addition to the variations in the atmospheric boundary layer (Garland and Derwent, 1979), O_3 is generated by the consumed VOCs and is sensitive to solar radiation variations (Lu et al., 2019). It should also be noted that in the early morning, both the concentrations of VOCs and NOx were sometimes relatively low, while the peak value of the O_3 concentration still frequently exceeded 74.6 ppbv. For example, the mean concentrations of NOx and VOCs were 21.8 ± 5.1 and 10.6 ± 1.4 ppbv, respectively, from 6:00 to 8:00 a.m. on August 1; while the 8 h-max O_3 concentration was 103 ± 5.9 ppbv with a mean wind speed of 0.84 m s^{-1}. Hence, it is difficult to directly connect the observed precursor concentrations to the O_3 pollution when the wind speed is low because the photochemistry results in the production of O_3 and the consumption of the precursors.

3.2. Measured and consumed concentrations and PICs of VOCs

During the observations, 51 VOCs were detected and classified into four categories, including 26 alkanes, 9 alkenes, 1 alkyne, and 15 aromatics. Fig. 3A–C shows the time series of the measured and consumed concentrations and the PICs of the VOCs, respectively. Fig. 3D–F shows the corresponding diurnal profiles, and Fig. 3G–I shows the relative contributions of these four types of VOCs.

The measured VOC concentrations ranged from 2.2 to 33.6 ppbv, with a mean value of 11.2 ± 5.7 ppbv. Compared to the same period (45.4 ± 15.2 ppbv) in August 2015 (Li et al., 2016), the concentration of VOCs in Beijing were effectively reduced. Moreover, the consumed VOCs and PICs varied from 0 to 52.3 ppbv and from 2.8 to 63.8 ppbv, with mean values of 3.4 ± 7.6 ppbv and 14.6 ± 8.4 ppbv, respectively. The measured concentration of VOCs was significantly lower than that of the PICs ($P < 0.05$; Table S2). The ratios of PICs to the measured concentration varied from 1 to 10.9, with a mean value of 1.5 ± 1.2. This suggests that more attention should be paid to the degradation of VOCs when discussing the formation of secondary pollutants via VOC oxidation.

As is shown in Fig. 3D, the measured VOCs exhibit a peak in the morning and evening and a minimum at noon due to the evolution of the mixing layer height (MLH), VOC emissions from traffic, and photochemical reactions of VOCs (Sarkar et al., 2016; Zhang et al., 2020a). This is consistent with the typical diurnal curves of VOCs observed previously (Li et al., 2016). However, the concentrations of the consumed VOCs exhibited an obvious increase in the daytime (Fig. 3E), which is similar to the diurnal variations in the consumed VOCs reported by Shao et al. (2011). This indicates that solar radiation and temperature

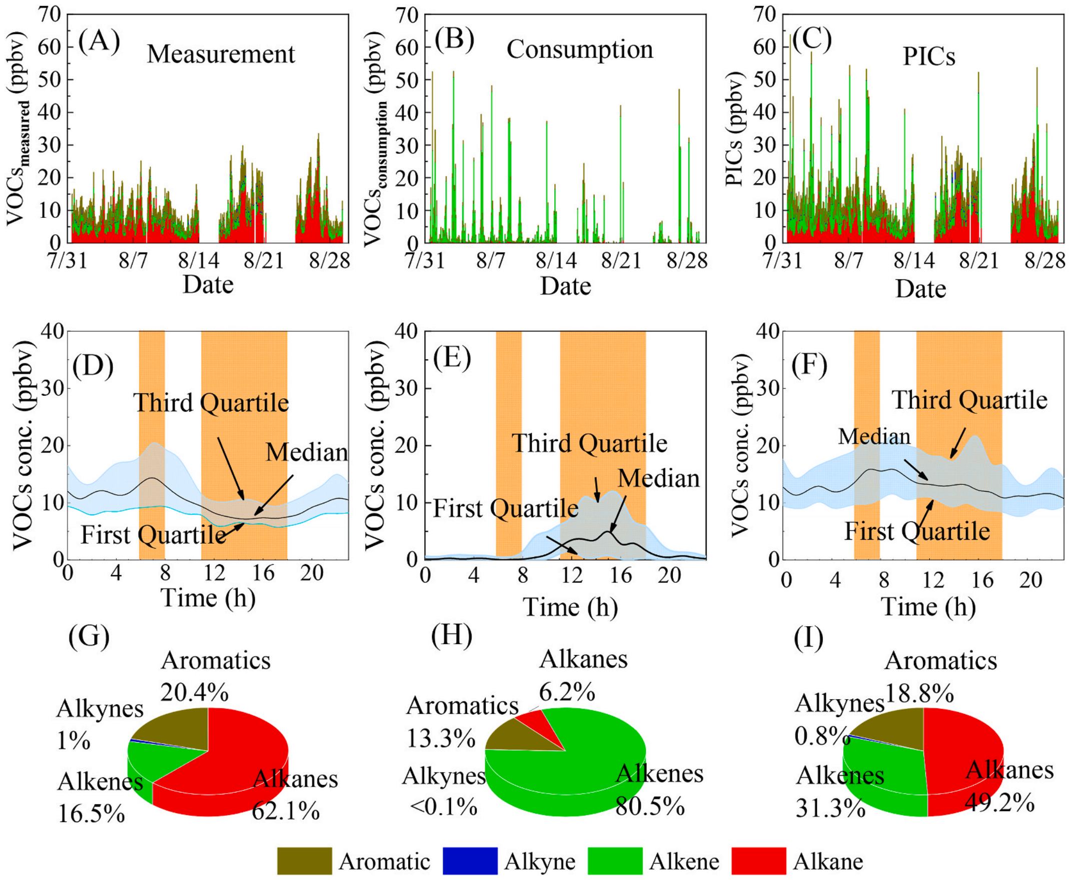

Fig. 3. Time series, diurnal curves, and percentages of (A, D, and G) measured; (B, E, and H) consumed; and (C, F, and I) photochemical initial concentrations of VOCs.

may play important roles in accelerating photochemical oxidation of VOCs (Rubin et al., 2006). The diurnal profile of the PICs (Fig. 3F) shows the combined effect of the measured and consumed concentrations, i.e., the PICs start to increase in the early morning and decreased slightly throughout the day until evening.

As is shown in Fig. 3G and I, alkanes were the most abundant species for both the measured VOCs and PICs, accounting for 62.1% of VOCs and 49.2% of PICs, respectively. However, in Fig. 3H, the alkenes account for 80.5% of the total consumed VOCs, followed by aromatics (13.3%), alkanes (6.2%), and alkynes (0.02%). It is well known that alkanes are important VOCs produced by vehicle exhaust and account for a large portion of the VOCs in the urban atmosphere (Song et al., 2019; Liu et al., 2020b). Moreover, fuel combustion also contributes to the ambient alkanes in the Beijing-Tianjin-Hebei (BTH) area (Guo et al., 2017). The concentration of alkanes is relatively high in many Chinese cities due to high emissions and the relatively low reactivity of alkanes (Cai et al., 2010; Mozaffar et al., 2020). Thus, alkanes were only underestimated by 6.3 ± 6.9% when photochemical reactions were taken into consideration (Table S3), which is much lower than those for alkenes (43.8 ± 30.2%) and aromatics (18.1 ± 18.2%) because they are more reactive with OH radicals. Gao et al. (2018) reported that the PIC of alkenes and aromatics in winter in the urban areas of Beijing increased from 16.8% to 22.3% and from 8.7% to 9.9% of the observed VOCs, respectively, compared with the measured concentrations. In our study, the alkenes and aromatics had higher proportions in suburban areas (Fig. 3I), accounting for 31.3% and 18.8%, respectively. This is ascribed to the stronger oxidation capacity in summer (i.e., in this study) than in winter (i.e., the study of Gao et al., 2018). As is shown in Fig. S3A, isoprene, propylene, and butene are highly reactive species in the consumed VOCs. This illustrates that the VOCs with high reactivity will react rapidly with OH radicals in suburban areas, resulting in apparent photochemical losses. Table S3 shows the details of the measured and consumed concentrations, the PICs and the average underestimated values for each species. Here, 12 species were underestimated by more than 30%. In particular, isoprene accounted for 67.9% of the consumed VOCs and 18.0% of the PICs. The PIC of isoprene was underestimated by 61.9%, which is slightly lower than that calculated by Shao et al. (2011) in the summer of 2008 (73%). Furthermore, as a critical biogenic VOC, isoprene has a high MIR (10.6 g g^{-1}) (Carter, 2010). Thus, the contribution of the biogenic VOCs to O_3 formation cannot be neglected in addition to anthropogenic VOC emissions (Song et al., 2019).

3.3. *Measurement-based OFP (OFP$_m$) vs. consumption-based OFP (OFP$_c$) and PICs-based OFP (OFP$_{PICs}$)*

Fig. 4A, C, and E show the time series of the OFP$_m$, the OFP$_c$ and the OFP$_{PICs}$ with mean values of 57.8 ± 26.3, 46.5 ± 109.9 and 103.9 ± 109.4 ppbv, respectively. It has been reported that the average OFP was about 135–164 ppbv near ground level in the BTH area (Geng et al., 2020), which is similar to our OFP$_{PICs}$ value. Although alkanes accounted for 62.1% of the total measured VOCs (Fig. 3G), they accounted for only 21.4% of the OFP$_m$ (Fig. 4B) due to the relatively small MIR values. In contrast, the alkenes and aromatics accounted for 36.6% and 41.9% of the OFP$_m$, respectively. The contribution of alkenes, aromatics, alkanes, and alkenes to OPF$_{PICs}$ was 56.8%, 30.3%, 12.8%, and 0.1%, respectively. As is shown in Fig. 4D and F, alkenes dominated the O_3 formation calculated using the consumed VOCs and the PICs. In addition, biogenic emissions were a major contributor to O_3 production (Fig. S3B). Isoprene accounted for 74.8% of the OFP$_c$, while its

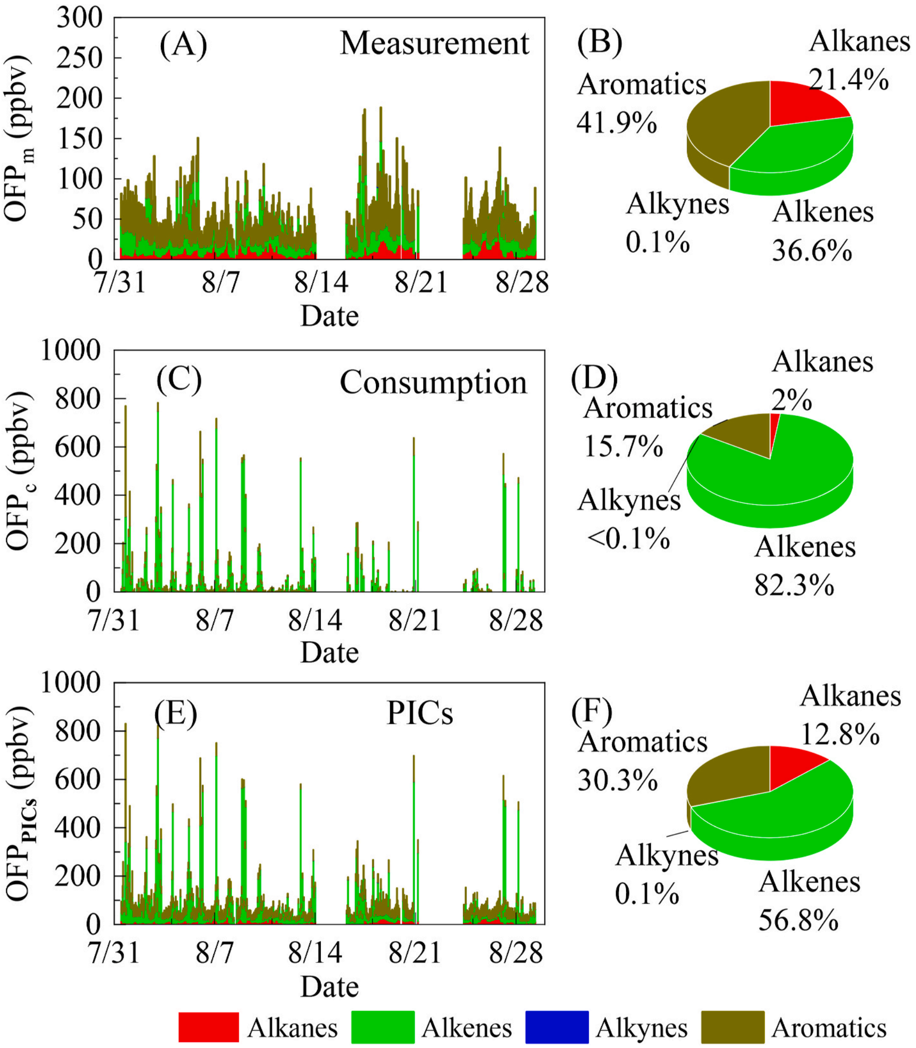

Fig. 4. Time series and percentages of (A, B) OFP$_m$, (C, D) OFP$_c$, (E, F) OFP$_{PICs}$.

contribution to the OFP$_{PICs}$ was 27.7%, which is comparable with the value (about 23%) reported by Xie et al. (2008) during the same period in downtown Beijing. In addition, several studies have found that propylene, trimethylbenzene, butene, and xylene produced by vehicle emissions, solvent use, and petrochemical plants are also important contributors to O_3 formation (Song et al., 2007; Liu et al., 2008).

Fig. 5 shows the relationship between the calculated OFPs and the observed O_3 concentrations. As is shown in Fig. 5A, the OFP$_m$ was slightly negatively correlated to the observed O_3 concentration (OFP$_m$ = 63.5–0.13 × c_{O3}, $R^2 = 0.32$), while the OFP$_m$ from 6:00 a.m. to 8:00 a.m. was positively correlated with the 8-h maximum O_3 concentration (OFP$_m$ = 0.68 × c_{O3}+13.7, $R^2 = 0.52$, Fig. S4). However, the VOCs were continuously oxidized to form O_3 during transport, leading to a continuous increase in the O_3 concentration. Thus, a linear correlation (OFP$_c$ = 1.24 × c_{O3}, $R^2 = 0.93$) was observed between the OFP$_c$ and the O_3 concentration in Fig. 5B. A linear response of the OFP$_{PICs}$ to the O_3 concentration was also observed (OFP$_{PICs}$ = 41.5 + 1.40 × c_{O3}, R^2 = 0.87, Fig. 5C). The slightly negative dependence of the OFP$_m$ on the observed O_3 concentration (Fig. 5A) may be resulted from the fact that more VOCs were consumed, or less VOCs were left when the O_3 level increased. These results imply that the OFP$_{PICs}$ or OFP$_c$ should more directly reflect the chemistry related to O_3 formation. Thus, the O_3 concentration can be predicted from the OFP$_{PICs}$ or OFP$_c$. This can be explained by the formation mechanism of tropospheric O_3 in the presence of VOCs. The production of O_3 is governed by photolysis of NO_2, while NO_2 is formed by the oxidation of NO by RO_2 and HO_2 without consumption of O_3. Both RO_2 and HO_2 should be positively correlated with the consumed VOCs rather than the measured VOCs. However, we

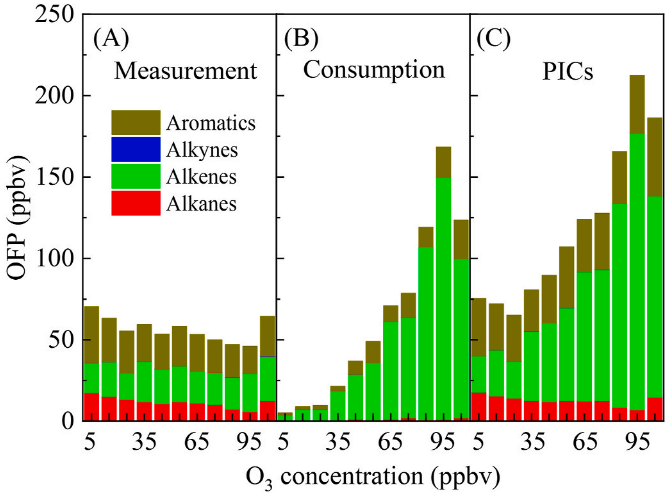

Fig. 5. Relationships between the OFPs and the binned O_3 concentrations. A) for OFP$_m$; B) for OFP$_c$; and C) for OFP$_{PICs}$.

consider the individual VOCs in isolation when calculating the OFP. The actual photochemical O_3 formation results from complex photochemical reactions in the atmosphere involving many VOC species and NO_x. Thus, competitive reactions between different VOCs and OH radicals cannot be reflected when we calculate the OFP using the measured VOCs, but it is accounted for when we calculate the OFP using the consumed VOCs or the chemical transport model and box model. Although the correlation between consumption-based OFP and O_3 concentration was slightly better than that of PIC-based OFP (Fig. 5), it is likely that the PIC-based OFP is more suitable for estimating O_3 pollution, as it reflects the maximum potential of O_3 formation in the atmosphere.

Box models are a powerful tool for understanding the chemical regimes of O_3 formation (Ehlers et al., 2016). To further understand the different relationships between the measured VOCs and PICs on O_3 formation, empirical kinetic modeling approach (EKMA) curves were derived based on box model simulations (Jenkin et al., 2017). As can be seen from Fig. 6, the O_3 production rate can be divided into three parts. The left-upper corner is a VOC-limited regime, while the right-lower corner is a NOx-limited regime. The area between the left-upper and right-lower corners is considered to be a transitional regime. In Fig. 6A, the measured VOCs and NO_x were used to assess the sensitivity of O_3 formation. The majority of the data resides in the VOC-limited zone, while a small amount of the data (in particular, for those datasets with O_3 concentrations of greater than 74.6 ppbv) resides in the transition regime. If we only consider the dataset measured in the early morning (Fig. S5), almost all of the data fall within the VOC-limited regime, with a VOCs/NOx ratio of 0.63 ± 0.53 (Fig. S5). This is consistent with previous work which found that O_3 formation is mainly VOC sensitive in Beijing (Li et al., 2020). When the PICs of the VOCs and NOx were taken into consideration, the sensitivity was significantly shifted toward the transitional and NO_x-limited regimes (Fig. 6B). As was discussed above, the consumed alkenes (especially isoprene) and aromatics mainly contributed to this large difference. Thus, the O_3 concentration is more sensitive to the PICs than to the measured VOCs. Our results suggest that it may be more reasonable to use the PICs-based values rather than the measured values to assess the sensitivity of O_3 production. However, more work is required to revisit the O_3 formation sensitivity in the future. In addition, more attention should be paid to the contribution of biogenic isoprene to O_3 formation in the summer in Beijing.

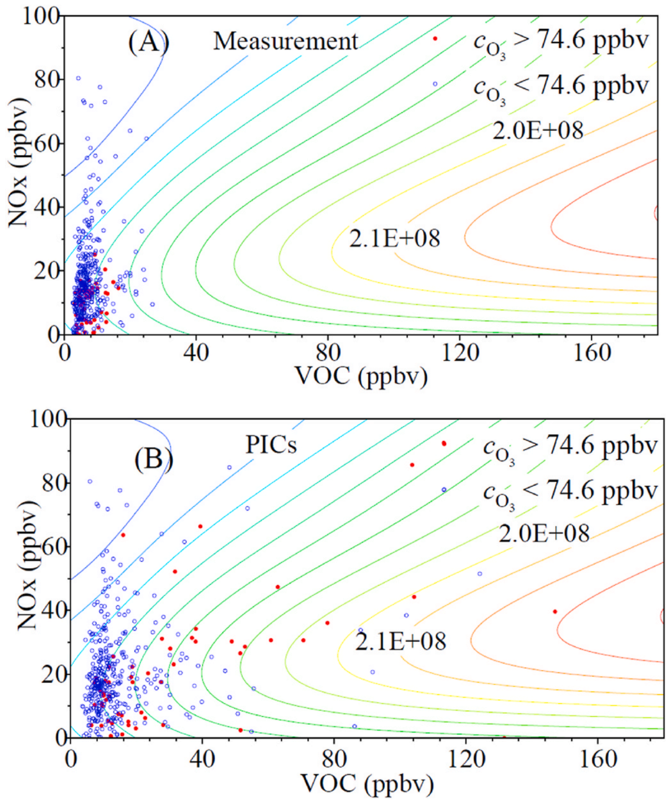

Fig. 6. EKMA curves of the ozone generation rate in summer in Beijing. A) for the measured concentrations of VOCs and NOx; B) for the PICs of VOCs and NOx.

3.4. *Measurement-based SOAP ($SOAP_m$) vs. consumption-based SOAP ($SOAP_c$) and PICs-based SOAP ($SOAP_{PICs}$)*

Fig. 7A shows the time series of the $SOAP_m$, which ranges from 1.9 to 22.5 μg m^{-3}, with a mean value of 8.4 ± 4.1 μg m^{-3}. It is similar to the SOAP value (7.7 μg m^{-3}) in the summer of 2016 in Beijing reported by Li et al. (2020). Aromatics were the most important contributor to the $SOAP_m$ (98.5%), followed by alkanes (0.8%) and alkenes (0.8%) (Fig. 7B). Similar to $SOAP_m$, the contribution of the aromatics to the $SOAP_c$ (1.9 ± 6.7 μg m^{-3}) was up to 92%, while the alkenes accounted for 7% (Fig. 7D). The aromatics, alkenes, and alkanes contribute 97.3%, 1.9%, and 0.8% to the $SOAP_{PICs}$ (10.3 ± 7.4 μg m^{-3}), respectively (Fig. 7F). Aromatics were the main contributors to $SOAP_{PICs}$, which is similar to the value of 98.2% reported by Li et al. (2020). The contributions of the alkenes to the SOAP in the source region were also underestimated when based on the measured VOCs, by about 67.7% for the alkenes (Table S4). The top 10 PICs-based species accounted for 81.8% of the total $SOAP_{PICs}$ (Fig. S3C). Toluene, benzene, and xylene were the important contributors to SOA formation (Kroll and Seinfeld, 2008), accounting for 60.4% of the total $SOAP_{PICs}$. In addition, the $SOAP_c/SOAP_{PICs}$ ratios for styrene and isoprene were 84.2 and 88%, respectively, due to consumption during transport. Thus, the contribution of these species to SOA formation cannot be ignored during observations. Photochemical loss is more important for estimating OFP than SOAP. This can be explained by the higher reactivity of alkenes than aromatics with OH radicals.

It should also be noted that the lifetimes ($1/k_2c_{OH}$) of highly reactive VOCs, such as isoprene and propene, greatly depend on the OH concentration. The daytime (8:00–17:00) OH concentrations ranged from 1.1 × 10^6 molecules cm^{-3} to 1.3 × 10^7 molecules cm^{-3}, with a mean value of 4.3 ± 3.1 × 10^6 molecules cm^{-3}, based on the modelled J_{O1D} using a previously described method (Liu et al., 2020a; Liu et al., 2020c). The corresponding photochemical ages were 0.01–16.9 h (1.7 ± 2.4 h). This value is comparable with previously reported photochemical ages (Shao et al., 2011; Gao et al., 2018) and indicates that the calculated PICs of highly reactive VOCs may be overestimated and should be taken as the upper limit. In addition, this method does not account for the transport of pollutants. Thus, while useful in a qualitatively sense, the method cannot quantitatively predict O_3 or SOA pollution. Although there are some uncertainties in estimating the photochemical age (Parrish et al., 2007), our results provide important information for evaluating the effects of photochemical processes on O_3 and SOA formation. It should be noted that O_3 also readily reacts with alkenes, leading to additional consumption of alkenes. However, when calculating the consumption of VOCs by O_3, similar to OH exposure, the O_3 exposure ($=c_{O3}\cdot t$) is required. The OH exposure is calculated from the changes in the VOC ratio using a pair of VOCs that are predominantly consumed by OH (Section 2.3). However, it is difficult to select an ideal pair of VOCs that are mainly consumed by O_3. As a result, we did not consider the contribution of O_3 to alkene consumption in this study, and further only measured biogenic isoprene emissions. This will lead to an underestimation of the contribution of the photochemical loss of VOCs to OFP and SOAP and suggests that other biogenic VOCs need to be investigated in the future.

4. Conclusions

In this study, we conducted measurements of air pollutants in the

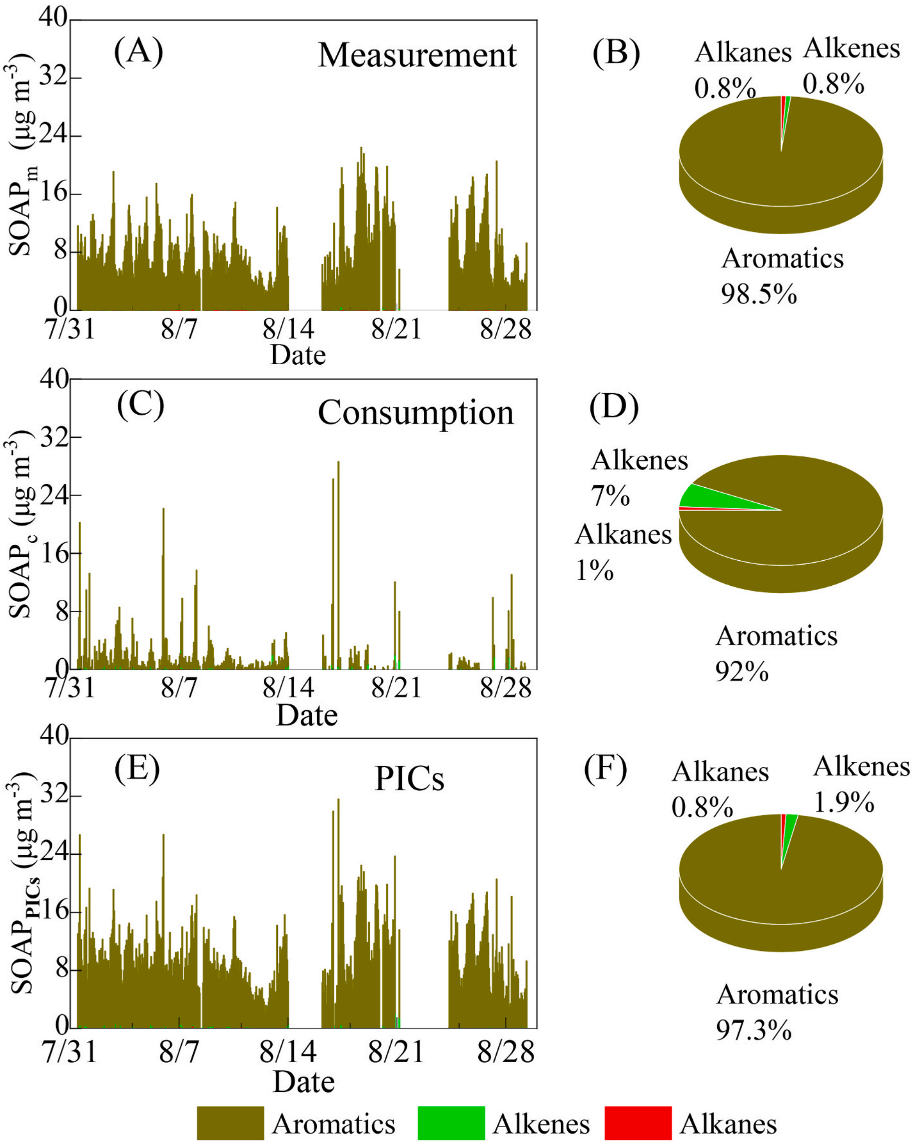

Fig. 7. Time series and percentages of (A, B) $SOAP_m$; (C, D) $SOAP_c$; and (E, F) $SOAP_{PICs}$.

southern suburbs of Beijing in August 2019. The OFP and SOAP were described based on the reactivity of VOCs. Of the detected 51 VOCs, the concentrations of alkenes and aromatics were underestimated by 43.8% and 18.1%, respectively, followed by alkanes (6.3%) and alkynes (1.4%). The alkenes and aromatics contributed 56.8% and 30.3% to the OFP_{PICs} respectively. The key species for O_3 formation were isoprene and propylene, and the main contributors to $SOAP_{PICs}$ were aromatics, accounting for 97.3%. The main species for SOA formation were toluene and xylene. The PICs-based OFPs were correlated with the observed O_3 concentrations, suggesting that the PICs-based OFPs can be used to predict O_3 concentrations. The O_3 formation shifted toward the transitional and NOx-limited regimes based on the PICs. Photochemical loss is more important for estimating OFP than SOAP because of the higher reactivity of alkenes than aromatics with OH radicals. In addition, it should be pointed out that only the isoprene from biogenic sources was measured, and it is necessary to assess the contribution of other biogenic VOCs to O_3 and SOA formation in the future.

Authorship attribution statement

Junlei Zhan: Methodology, Data curation, Writing - original draft. **Zeming Feng**: Methodology, Investigation, Data curation. **Pengfei Liu:** Methodology, Data curation, Writing - review & editing. **Xiaowei He**: Methodology, Investigation, Data curation. **Zhouming He:** Methodology, Investigation, Data curation. **Tianzeng Chen:** Methodology, Investigation, Data curation. **Yafei Wang:** Methodology, Investigation, Resources, Data curation, Writing - review & editing. **Hong He:** Writing - review & editing. **Yujing Mu:** Methodology, Writing - review & editing. **Yongchun Liu**: Conceptualization, Methodology, Data curation, Writing - review & editing.

Declaration of competing interest

The authors declare that they have no known competing financial interests or personal relationships that could have appeared to influence the work reported in this paper.

Acknowledgments

This research was financially supported by the National Natural Science Foundation of China (41877306, 21976190, 21806011), the Ministry of Science and Technology of the People's Republic of China (2019YFC0214701), Chinese Academy of Sciences (RCEES-CYZX-2020-02) and Beijing University of Chemical Technology. We thank Wei Ma, Yifei Song, Chengtang Liu, Qinxing Ma and Kang Yang for operating some of the instruments during campaign studies. We thank Junfeng Liu and Jiannong Quan for their instructive suggestions on data process and preparing the manuscript. We also thank LetPub (www.letpub.com) and Dr. John Liggio for its linguistic assistance during the preparation of this manuscript.

Appendix A. Supplementary data

Supplementary data to this article can be found online at https://doi.org/10.1016/j.envpol.2021.117444.

References

Alvim, D.S., Gatti, L.V., Corrêa, S.M., Chiquetto, J.B., Santos, G.M., de Souza Rossatti, C., Pretto, A., Rozante, J.R., Figueroa, S.N., Pendharkar, J., Nobre, P., 2018. Determining VOCs reactivity for ozone forming potential in the megacity of são paulo. Aerosol Air Qual. Res. 18, 2460–2474.

Atkinson, R., Arey, J., 2003. Atmospheric degradation of volatile organic compounds. Chem. Rev. 103, 4605–4638.

Bertman, S.B., Roberts, J.M., Parrish, D.D., Buhr, M.P., Goldan, P.D., Kuster, W.C., Fehsenfeld, F.C., Montzka, S.A., Westberg, H., 1995. Evolution of alkyl nitrates with air mass age. J. Geophys. Res. Atmos. 100, 22805–22813.

Cai, C., Geng, F., Tie, X., Yu, Q., An, J., 2010. Characteristics and source apportionment of VOCs measured in Shanghai, China. Atmos. Environ. 44, 5005–5014.

Carter, W., 2010. Updated maximum incremental reactivity scale and hydrocarbon bin reactivities for regulatory applications. California Air Resources Board Contract, 1, pp. 7–339.

Chameides, W., Fehsenfeld, F., Rodgers, M., Cardelino, C., Martinez, J., Parrish, D., Lonneman, W., Lawson, D., Rasmussen, R., Zimmerman, P., 1992. Ozone precursor relationships in the ambient atmosphere. J. Geophys. Res. Atmos. 97, 6037–6055.

Chen, T., Liu, J., Liu, Y., Ma, Q., Ge, Y., Zhong, C., Jiang, H., Chu, B., Zhang, P., Ma, J., Liu, P., Wang, Y., Mu, Y., He, H., 2020. Chemical characterization of submicron aerosol in summertime Beijing: a case study in southern suburbs in 2018. Chemosphere 247, 125918.

Cheng, N., Chen, Z., Sun, F., Sun, R., Dong, X., Xie, X., Xu, C., 2018. Ground ozone concentrations over Beijing from 2004 to 2015: variation patterns, indicative precursors and effects of emission-reduction. Environ. Pollut. 237, 262–274.

Derwent, R.G., Jenkin, M.E., Utembe, S.R., Shallcross, D.E., Murrells, T.P., Passant, N.R., 2010. Secondary organic aerosol formation from a large number of reactive man-made organic compounds. Sci. Total Environ. 408, 3374–3381.

Duan, J., Huang, R.J., Li, Y., Chen, Q., Zheng, Y., Chen, Y., Lin, C., Ni, H., Wang, M., Ovadnevaite, J., Ceburnis, D., Chen, C., Worsnop, D.R., Hoffmann, T., O'Dowd, C., Cao, J., 2020. Summertime and wintertime atmospheric processes of secondary aerosol in Beijing. Atmos. Chem. Phys. 20, 3793–3807.

Ehlers, C., Klemp, D., Rohrer, F., Mihelcic, D., Wegener, R., Kiendler-Scharr, A., Wahner, A., 2016. Twenty years of ambient observations of nitrogen oxides and specified hydrocarbons in air masses dominated by traffic emissions in Germany. Faraday Discuss 189, 407–437.

Gao, J., Zhang, J., Li, H., Li, L., Xu, L., Zhang, Y., Wang, Z., Wang, X., Zhang, W., Chen, Y., Cheng, X., Zhang, H., Peng, L., Chai, F., Wei, Y., 2018. Comparative study of volatile organic compounds in ambient air using observed mixing ratios and initial mixing ratios taking chemical loss into account – a case study in a typical urban area in Beijing. Sci. Total Environ. 628–629, 791–804.

Gao, Y., Li, M., Wan, X., Zhao, X., Wu, Y., Liu, X., Li, X., 2021. Important contributions of alkenes and aromatics to VOCs emissions, chemistry and secondary pollutants formation at an industrial site of central eastern China. Atmos. Environ. 244, 117927.

Garland, J.A., Derwent, R.G., 1979. Destruction at the ground and the diurnal cycle of concentration of ozone and other gases. Q. J. Roy. Meteorol. Soc. 105, 169–183.

Geng, C., Wang, J., Yin, B., Zhao, R., Li, P., Yang, W., Xiao, Z., Li, S., Li, K., Bai, Z., 2020. Vertical distribution of volatile organic compounds conducted by tethered balloon in the Beijing-Tianjin-Hebei region of China. J. Environ. Sci. 95, 121–129.

Guo, H., Ling, Z.H., Cheng, H.R., Simpson, I.J., Lyu, X.P., Wang, X.M., Shao, M., Lu, H.X., Ayoko, G., Zhang, Y.L., Saunders, S.M., Lam, S.H.M., Wang, J.L., Blake, D.R., 2017. Tropospheric volatile organic compounds in China. Sci. Total Environ. 574, 1021–1043.

Han, D., Wang, Z., Cheng, J., Wang, Q., Chen, X., Wang, H., 2017. Volatile organic compounds (VOCs) during non-haze and haze days in Shanghai: characterization and secondary organic aerosol (SOA) formation. Environ. Sci. Pollut. Res. 24, 18619–18629.

Jenkin, M.E., Derwent, R.G., Wallington, T.J., 2017. Photochemical ozone creation potentials for volatile organic compounds: rationalization and estimation. Atmos. Environ. 163, 128–137.

Jimenez, J.L., Canagaratna, M., Donahue, N., Prevot, A., Zhang, Q., Kroll, J.H., DeCarlo, P.F., Allan, J.D., Coe, H., Ng, N., 2009. Evolution of organic aerosols in the atmosphere. Science 326, 1525–1529.

Krizan, P., Miksovsky, J., Kozubek, M., Gengchen, W., Jianhui, B., 2011. Long term variability of total ozone yearly minima and maxima in the latitudinal belt from 20°N to 60°N derived from the merged satellite data in the period 1979–2008. Adv. Space Res. 48, 2016–2022.

Kroll, J.H., Seinfeld, J.H., 2008. Chemistry of secondary organic aerosol: formation and evolution of low-volatility organics in the atmosphere. Atmos. Environ. 42, 3593–3624.

Kumar, A., Singh, D., Kumar, K., Singh, B.B., Jain, V.K., 2018. Distribution of VOCs in urban and rural atmospheres of subtropical India: temporal variation, source attribution, ratios, OFP and risk assessment. Sci. Total Environ. 613, 492–501.

Li, J., Wu, R., Li, Y., Hao, Y., Xie, S., Zeng, L., 2016. Effects of rigorous emission controls on reducing ambient volatile organic compounds in Beijing, China. Sci. Total Environ. 557, 531–541.

Li, Q., Su, G., Li, C., Liu, P., Zhao, X., Zhang, C., Sun, X., Mu, Y., Wu, M., Wang, Q., Sun, B., 2020. An investigation into the role of VOCs in SOA and ozone production in Beijing, China. Sci. Total Environ. 720, 137536.

Li, H., Ma, Y., Duan, F., Zhu, L., Ma, T., Yang, S., Xu, Y., Li, F., Huang, T., Kimoto, T., Zhang, Q., Tong, D., Wu, N., Hu, Y., Huo, M., Zhang, Q., Ge, X., Gong, W., He, K., 2021. Stronger secondary pollution processes despite decrease in gaseous precursors: a comparative analysis of summer 2020 and 2019 in Beijing. Environ. Pollut. 279, 116923.

Liu, C., Mu, Y., Zhang, C., Zhang, Z., Zhang, Y., Liu, J., Sheng, J., Quan, J., 2016. Development of gas chromatography-flame ionization detection system with a single column and liquid nitrogen-free for measuring atmospheric C2–C12 hydrocarbons. J. Chromatogr. A 1427, 134–141.

Liu, Y., Ni, S., Jiang, T., Xing, S., Zhang, Y., Bao, X., Feng, Z., Fan, X., Zhang, L., Feng, H., 2020a. Influence of Chinese new year overlapping COVID-19 lockdown on HONO sources in shijiazhuang. Sci. Total Environ. 745, 141025.

Liu, Y., Shao, M., Fu, L., Lu, S., Zeng, L., Tang, D., 2008. Source profiles of volatile organic compounds (VOCs) measured in China: Part I. Atmos. Environ. 42, 6247–6260.

Liu, Y., Song, M., Liu, X., Zhang, Y., Hui, L., Kong, L., Zhang, Y., Zhang, C., Qu, Y., An, J., Ma, D., Tan, Q., Feng, M., 2020b. Characterization and sources of volatile organic compounds (VOCs) and their related changes during ozone pollution days in 2016 in Beijing, China. Environ. Pollut. 257, 113599.

Liu, Y., Zhang, Y., Lian, C., Yan, C., Feng, Z., Zheng, F., Fan, X., Chen, Y., Wang, W., Chu, B., Wang, Y., Cai, J., Du, W., Daellenbach, K.R., Kangasluoma, J., Bianchi, F., Kujansuu, J., Petäjä, T., Wang, X., Hu, B., Wang, Y., Ge, M., He, H., Kulmala, M., 2020c. The promotion effect of nitrous acid on aerosol formation in wintertime in Beijing: the possible contribution of traffic-related emissions. Atmos. Chem. Phys. 20, 13023–13040.

Lu, X., Zhang, L., Chen, Y., Zhou, M., Zheng, B., Li, K., Liu, Y., Lin, J., Fu, T.M., Zhang, Q., 2019. Exploring 2016–2017 surface ozone pollution over China: source contributions and meteorological influences. Atmos. Chem. Phys. 19, 8339–8361.

Ma, R., Ban, J., Wang, Q., Zhang, Y., Yang, Y., He, M.Z., Li, S., Shi, W., Li, T., 2021. Random forest model based fine scale spatiotemporal O_3 trends in the Beijing-Tianjin-Hebei region in China, 2010 to 2017. Environ. Pollut. 276, 116635.

Maji, K.J., Li, V.O.K., Lam, J.C.K., 2020. Effects of China's current Air Pollution Prevention and Control Action Plan on air pollution patterns, health risks and mortalities in Beijing 2014–2018. Chemosphere 260, 127572.

Makar, P.A., Fuentes, J.D., Wang, D., Staebler, R.M., Wiebe, H.A., 1999. Chemical processing of biogenic hydrocarbons within and above a temperate deciduous forest. J. Geophys. Res. Atmos. 104, 3581–3603.

Mozaffar, A., Zhang, Y.-L., Fan, M., Cao, F., Lin, Y.-C., 2020. Characteristics of summertime ambient VOCs and their contributions to O_3 and SOA formation in a suburban area of Nanjing, China. Atmos. Res. 240, 104923.

Odum, J.R., Jungkamp, T.P.W., Griffin, R.J., Flagan, R.C., Seinfeld, J.H., 1997. The atmospheric aerosol-forming potential of whole gasoline vapor. Science 276, 96–99.

Parrish, D.D., Stohl, A., Forster, C., Atlas, E.L., Blake, D.R., Goldan, P.D., Kuster, W.C., de Gouw, J.A., 2007. Effects of mixing on evolution of hydrocarbon ratios in the troposphere. J. Geophys. Res. Atmos. 112, D10S34.

Roberts, J.M., Fehsenfeld, F.C., Liu, S.C., Bollinger, M.J., Hahn, C., Albritton, D.L., Sievers, R.E., 1984. Measurements of aromatic hydrocarbon ratios and NOx concentrations in the rural troposphere: observation of air mass photochemical aging and NOx removal. Atmos. Environ. 18, 2421–2432.

Rubin, J.I., Kean, A.J., Harley, R.A., Millet, D.B., Goldstein, A.H., 2006. Temperature dependence of volatile organic compound evaporative emissions from motor vehicles. J. Geophys. Res. Atmos. 111, D03305.

Sarkar, C., Sinha, V., Kumar, V., Rupakheti, M., Panday, A., Mahata, K.S., Rupakheti, D., Kathayat, B., Lawrence, M.G., 2016. Overview of VOC emissions and chemistry from PTR-TOF-MS measurements during the SusKat-ABC campaign: high acetaldehyde, isoprene and isocyanic acid in wintertime air of the Kathmandu Valley. Atmos. Chem. Phys. 16, 3979–4003.

Shao, M., Bin, W., Sihua, L., Bin, Y., Ming, W., 2011. Effects of beijing Olympics control measures on reducing reactive hydrocarbon species. Environ. Sci. Technol. 45, 514–519.

Song, C., Liu, B., Dai, Q., Li, H., Mao, H., 2019. Temperature dependence and source apportionment of volatile organic compounds (VOCs) at an urban site on the north China plain. Atmos. Environ. 207, 167–181.

Song, Y., Shao, M., Liu, Y., Lu, S., Kuster, W., Goldan, P., Xie, S., 2007. Source apportionment of ambient volatile organic compounds in beijing. Environ. Sci. Technol. 41, 4348–4353.

Streets, D.G., Fu, J.S., Jang, C.J., Hao, J., He, K., Tang, X., Zhang, Y., Wang, Z., Li, Z., Zhang, Q., Wang, L., Wang, B., Yu, C., 2007. Air quality during the 2008 beijing olympic games. Atmos. Environ. 41, 480–492.

Tan, Z., Lu, K., Jiang, M., Su, R., Dong, H., Zeng, L., Xie, S., Tan, Q., Zhang, Y., 2018. Exploring ozone pollution in Chengdu, southwestern China: a case study from radical chemistry to O_3-VOC-NOx sensitivity. Sci. Total Environ. 636, 775–786.

Tang, G., Li, X., Wang, Y., Xin, J., Ren, X., 2009. Surface ozone trend details and interpretations in Beijing, 2001–2006. Atmos. Chem. Phys. 9, 8813–8823.

Wang, B., Shao, M., Lu, S.H., Yuan, B., Zhao, Y., Wang, M., Zhang, S.Q., Wu, D., 2010. Variation of ambient non-methane hydrocarbons in Beijing city in summer 2008. Atmos. Chem. Phys. 10, 5911–5923.

Warneke, C., de Gouw, J.A., Goldan, P.D., Kuster, W.C., Williams, E.J., Lerner, B.M., Jakoubek, R., Brown, S.S., Stark, H., Aldener, M., Ravishankara, A.R., Roberts, J.M., Marchewka, M., Bertman, S., Sueper, D.T., McKeen, S.A., Meagher, J.F., Fehsenfeld, F.C., 2004. Comparison of daytime and nighttime oxidation of biogenic and anthropogenic VOCs along the new england coast in summer during new england air quality study 2002. J. Geophys. Res. Atmos. 109, D10309.

Wu, S., Tang, G., Wang, Y., Yang, Y., Yao, D., Zhao, W., Gao, W., Sun, J., Wang, Y., 2020. Vertically decreased VOC concentration and reactivity in the planetary boundary layer in winter over the North China Plain. Atmos. Res. 240, 104930.

Wu, J., Wang, Y., Liang, J., Yao, F., 2021. Exploring common factors influencing $PM_{2.5}$ and O_3 concentrations in the Pearl River Delta: tradeoffs and synergies. Environ. Pollut. 285, 117138.

Xie, X., Shao, M., Liu, Y., Lu, S., Chang, C.-C., Chen, Z.-M., 2008. Estimate of initial isoprene contribution to ozone formation potential in Beijing, China. Atmos. Environ. 42, 6000–6010.

Yuan, B., Hu, W.W., Shao, M., Wang, M., Chen, W.T., Lu, S.H., Zeng, L.M., Hu, M., 2013. VOC emissions, evolutions and contributions to SOA formation at a receptor site in eastern China. Atmos. Chem. Phys. 13, 8815–8832.

Zhang, F., Shang, X., Chen, H., Xie, G., Fu, Y., Wu, D., Sun, W., Liu, P., Zhang, C., Mu, Y., Zeng, L., Wan, M., Wang, Y., Xiao, H., Wang, G., Chen, J., 2020a. Significant impact of coal combustion on VOCs emissions in winter in a North China rural site. Sci. Total Environ. 720, 137617.

Zhang, K., Xu, J., Huang, Q., Zhou, L., Fu, Q., Duan, Y., Xiu, G., 2020b. Precursors and potential sources of ground-level ozone in suburban Shanghai. Front. Environ. Sci. Eng. 14, 92.

Zhang, L., Wang, T., Zhang, Q., Zheng, J., Xu, Z., Lv, M., 2016. Potential sources of nitrous acid (HONO) and their impacts on ozone: a WRF-Chem study in a polluted subtropical region. J. Geophys. Res. Atmos. 121, 3645–3662.

Zhang, Z., Zhang, X., Gong, D., Quan, W., Zhao, X., Ma, Z., Kim, S.-J., 2015. Evolution of surface O_3 and $PM_{2.5}$ concentrations and their relationships with meteorological conditions over the last decade in Beijing. Atmos. Environ. 108, 67–75.

Zheng, H., Kong, S., Chen, N., Niu, Z., Zhang, Y., Jiang, S., Yan, Y., Qi, S., 2021. Source apportionment of volatile organic compounds: implications to reactivity, ozone formation, and secondary organic aerosol potential. Atmos. Res. 249, 105344.